INTERNATIONAL JOURNAL FOR NUMERICAL METHODS IN FLUIDS
Int. J. Numer. Meth. Fluids 2005; **48**:1–16
Published online 29 December 2004 in Wiley InterScience (www.interscience.wiley.com). DOI: 10.1002/fld.815

On Marangoni effects in a heated thin fluid layer with a monolayer surfactant. Part I: model development and stability analysis

Xiaowen Wang and Graham F. Carey*,†

The University of Texas at Austin, U.S.A.

SUMMARY

We develop a model for surface tension driven flow induced by an insoluble surfactant monolayer on a heated thin fluid layer. The mathematical model is based on a perturbation analysis for a thin fluid layer. The resulting model involves coupling of flow and heat transfer to an additional transport equation for surfactant concentration on the surface. We develop the stability analysis of this coupled system. We characterize the stability behaviour and induced wave motion into four parametric regions based on linear stability analysis. A finite element formulation and numerical studies of the behaviour in the various stability regimes are given in Part II. Copyright © 2004 John Wiley & Sons, Ltd.

KEY WORDS: surfactant surface tension; stability analysis; finite elements

1. INTRODUCTION

Surface tension is an important localized property that arises on the interface between two immiscible fluids or at a fluid–gas interface and can be attributed to unbalanced molecular 'attraction' which tends to pull molecules into the interior of a liquid phase, and hence to minimize the surface area [1]. This results in a higher potential energy for the molecules at the interface. Consequently the interface tends to contract to reduce the interface area in order to minimize the potential energy, as if it were in a state of tension like a stretched membrane [2]. Surface tension is represented as the magnitude of the force per unit length normal to a cut in the interface, or the free energy per unit area. Both thermocapillary and surfactant effects at the interface can induce flow through associated shear stresses. These Marangoni flows arise in many diverse application areas such as coating, electronic cooling, wafer drying, biofluidic chip fabrication and medicine delivery.

It has long been recognized that thermocapillary Marangoni effects are a cause of convection instability in thin fluid layers [3–9]. In this study we focus on the long wavelength solution and

*Correspondence to: G. F. Carey, The University of Texas at Austin, U.S.A.
†E-mail: carey@cfdlab.ae.utexas.edu

Received 11 August 2003
Revised 18 October 2004

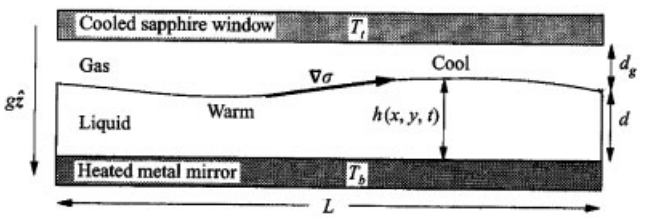

Figure 1. Sketch of a surface-tension driven Marangoni convection in a thin film heated from below. Since surface tension decreases with increased temperature, the temperature variations generate surface tension gradients, which can initiate fluid flow (from Reference [4]).

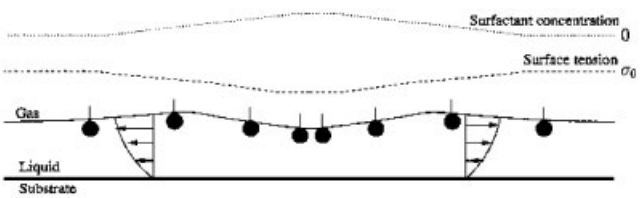

Figure 2. Illustration of surfactant capillary effect (from Reference [16]).

related instability. Figure 1 is a sketch of the long wavelength instability experiment studied in References [4, 5, 10]. The temperature difference applied between the top and bottom plates in Figure 1 builds up vertical temperature gradients in the liquid and gas layers, which induce surface tension gradients on the interface when it is perturbed away from the horizontal profile. Because surface tension increases with decreased temperature, the interface regions with higher elevations are subject to stronger surface tension and hence are pulled further toward the top cool plate. Thus in this experiment the Marangoni effect tends to destabilize the interface profile and leads to the long wavelength instability. Further details on the experiment and theoretical analysis can be found in References [4, 5, 10]. A finite element study of the thermocapillarity problem is presented in Reference [11].

One approach to stabilizing the free surface is to introduce a surfactant monolayer on the surface. The schematic in Figure 2 illustrates how surfactant capillarity affects the fluid flow. Assume the surfactant concentration is higher in the middle region, as shown in the figure. Because the surface tension is lower when the concentration is higher [1], the surface tension is lower in the middle region and increases towards the ends. This surface tension gradient then induces an outgoing Marangoni flow. Now let us imagine instead that we have an initial uniform layer with uniform surfactant distribution on the surface. Let some external factor (e.g. a non-uniform pressure) depress the middle region of the interface. This gives rise to an outgoing flow and surfactant molecules are then convected towards the ends, leading to a lower concentration in the middle. Because surface tension is higher when the concentration is lower, the surface tension in the middle will be higher than at the ends. This surface tension gradient then tends to pull back the surfactant molecules towards the middle and stabilizes the system.

The calming effect of surfactant on wave motion was known in antiquity and sailors were advised to pour oil on troubled waters (e.g. see Reference [9]). A surfactant can damp wave

motions throughout the wave spectrum from short capillary waves up to long gravity waves. The damping takes effect by modifying the normal and shear stresses on the surface. Solubility of the surfactant lessens its damping effect, particularly for the long wavelengths. The analysis in Reference [9] assumes the surfactant covers the entire surface area, whereas some more recent research has investigated surfactant spreading with an initial concentration front [12]. Experimentally and theoretically, it has been shown that surfactants spreading on a thin liquid film will drive fluid into a thickened and rapidly advancing ridge with subsequent thinning near the original line of contact between the clean surface and surfactant sub-regions [17]. For ultrathin liquid films (100–1000 Å), the van der Waals force becomes important and may lead to a rupture instability (see, e.g. Reference [18] for a review). In VanHook's experiment [5], the average film thickness is ~ 0.125 mm, so van der Waals forces can thus be safely neglected if the solution is far away from a dry spot.

In the next section we first consider the surfactant constitutive properties and derive the governing equations for the surface elevation and the surfactant concentration. Then we perform a linear stability analysis and accordingly categorize the parametric space in terms of (ε_q, D_s), where ε_q is the non-dimensional stability control parameter and D_s is the inverse dynamic Bond number for solutocapillarity. Numerical results in 1D and 2D for coupled thermocapillarity and solutocapillarity in different parametric categories are presented in Part II and the results are related to a linear stability analysis developed here in Part I.

2. MATHEMATICAL MODEL

2.1. Surfactant constitutive relation

First, we introduce two different non-dimensionalizations of the surface tension to serve different purposes. The first one is [13]

$$\sigma \equiv \frac{\sigma^{\mathrm{p}}}{\sigma^{\mathrm{p}}_{\mathrm{eq}}} \tag{1}$$

and is used primarily in the constitutive model, which describes the correlation between the surface tension and the surfactant concentration. The second one is

$$S = \frac{\sigma^{\mathrm{p}}}{\rho \nu \kappa / d} = \frac{\sigma^{\mathrm{p}}_{\mathrm{eq}}}{\rho \nu \kappa / d} \frac{\sigma^{\mathrm{p}}}{\sigma^{\mathrm{p}}_{\mathrm{eq}}} = S_{\mathrm{eq}} \sigma \tag{2}$$

where ρ, ν, κ and d are density, dynamic viscosity, thermal diffusivity and average depth of the liquid respectively. This definition is used in the governing equation for the surfactant concentration. (In the above expressions, we use the superscript p to distinguish the physical quantity from the non-dimensional quantity. Also we use subscripts eq and ∞ to denote the quantity at the equilibrium state and the saturation state, respectively).

We adopt the constitutive model used in References [13–15], which describes a non-linear correlation between the non-dimensionalized surface tension and surfactant concentration

$$\sigma = \sigma_0 + E \ln(1 - \alpha \Gamma) \tag{3}$$

where $\sigma_0 \equiv \sigma^{\mathrm{p}}_0 / \sigma^{\mathrm{p}}_{\mathrm{eq}}$, $E \equiv RT^{\mathrm{p}} \Gamma^{\mathrm{p}}_{\infty} / \sigma^{\mathrm{p}}_{\mathrm{eq}}$, $\alpha \equiv \Gamma^{\mathrm{p}}_{\mathrm{eq}} / \Gamma^{\mathrm{p}}_{\infty}$, $\Gamma \equiv \Gamma^{\mathrm{p}} / \Gamma^{\mathrm{p}}_{\mathrm{eq}}$, σ^{p}_0 is the surface tension at zero surfactant concentration (σ^{p}_0 is temperature dependent), R is the ideal gas constant, T^{p} is the

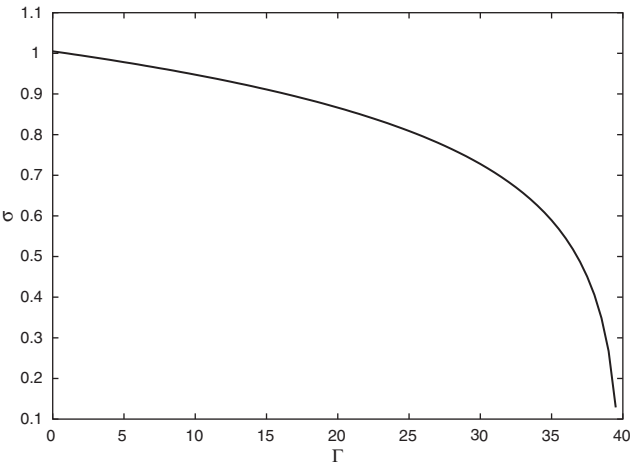

Figure 3. σ versus Γ for $E = 0.2$ and $\alpha = 2.5\%$.

temperature, E is a dimensionless parameter measuring the sensitivity of surface tension to the local surfactant concentration, and α is the fraction of the interfacial area that is initially covered by surfactant. In later numerical studies we use the value $E = 0.2$ [13]. Setting $\Gamma = 1$ in (3) gives $\sigma_0 = \sigma(\Gamma = 1) - E\ln(1-\alpha) = 1 - E\ln(1-\alpha)$. Thus we may rewrite (3) as

$$\sigma = 1 + E\ln\left(\frac{1-\alpha\Gamma}{1-\alpha}\right) \tag{4}$$

which implies that the valid ranges for σ and Γ are

$$0 \leqslant \sigma \leqslant \sigma_0 = 1 - E\ln(1-\alpha), \quad 0 \leqslant \Gamma \leqslant 1/\alpha = \Gamma^{\mathrm{p}}_{\infty}/\Gamma^{\mathrm{p}}_{\mathrm{eq}} \tag{5}$$

This constitutive model covers a wide range of Γ values, from dilute ($\Gamma^{\mathrm{p}} \ll \Gamma^{\mathrm{p}}_{\infty}$) to near saturation ($\Gamma^{\mathrm{p}} \to \Gamma^{\mathrm{p}}_{\infty}$). For $\Gamma^{\mathrm{p}} \ll \Gamma^{\mathrm{p}}_{\infty}$, the surface velocity can easily convect surfactant to form large surfactant concentration gradients and thus strongly affect the surface tension. For Γ^{p} near $\Gamma^{\mathrm{p}}_{\infty}$, the stresses resisting accumulation of surfactant are large and act to prevent the local concentration Γ^{p} from reaching $\Gamma^{\mathrm{p}}_{\infty}$, which is a logarithmic singular point in the constitutive model (4). Thus Γ^{p} may only deviate slightly from a uniform distribution and the surface tension is high. In the current study, we focus on the dilute concentration case in the presence of thermocapillarity where surfactant is easily advected.

Figure 3 shows a plot of the relationship between σ and Γ used in later simulations with $E = 0.2$ and $\alpha = 0.025$. It follows that $\Gamma = 1/\alpha = 40$ is the logarithmic singular point. When Γ is far away from $1/\alpha$, the relationship is near linear and a linearization of the model will be sufficient for modelling problems with Γ in this range. When $\alpha \to 1$, the singular point $\Gamma = 1/\alpha \to 1$. Note that $\Gamma = 1$ corresponds to the equilibrium concentration. This implies that when the surfactant is near fully packed on the surface, the valid range of Γ is almost completely in the logarithmic non-linear range, and thus the full non-linear constitutive model should be used.

2.2. Surfactant transport

The governing equation for the surfactant concentration is [14]

$$\frac{\partial \Gamma}{\partial t} + \nabla_s \cdot (\boldsymbol{V}_s \Gamma) + \left(\frac{1}{R_1} + \frac{1}{R_2}\right) \Gamma V_n - \kappa_s \nabla^2 \Gamma = 0 \tag{6}$$

where R_1 and R_2 are local radii of curvature of the interface, $\boldsymbol{V}_s$ and V_n are the tangential and normal components of the velocity at the interface, and κ_s is the surface diffusivity. Note that in this model we set the mass flux j_n (discussed in Reference [14]) to zero because only the insoluble monolayer limit is of interest here; that is, we assume the mass transfer is slow compared to surface convection. This is the same approach as used in Reference [15].

This model can be simplified for the layer case of interest here as follows. First, we scale the spatial co-ordinates by d, time by d^2/κ, velocity by κ/d, so that (6) becomes

$$\frac{\partial \Gamma}{\partial t} + \nabla_s \cdot (\boldsymbol{V}_s \Gamma) + \left(\frac{1}{R_1} + \frac{1}{R_2}\right) \Gamma V_n - \frac{1}{Pe_s} \nabla^2 \Gamma = 0 \tag{7}$$

where $Pe_s \equiv \kappa/\kappa_s$ is the surface Peclet number.

We make the same long wavelength assumption as used in deriving the thermocapillary model in References [4, 11] and again expand in the fundamental wavevector $q \equiv 2\pi d/L \ll 1$. Using $\partial/\partial t \sim O(q)$, $\partial/\partial x$, $\partial/\partial y \sim O(q)$, $\partial^2/\partial x^2$, $\partial^2/\partial y^2$, $\partial^2/\partial x \partial y \sim O(q^2)$, $\boldsymbol{V}_s \sim O(1)$, $V_n \sim O(q)$, $\Gamma \sim O(1)$, the dilatation term and the surface diffusion term are $O(q^3)$ and $O(q^2)$, respectively. Thus, the leading order ($O(q)$) terms in the expansion based on q satisfy

$$\frac{\partial \Gamma}{\partial t} + \nabla_s \cdot (\boldsymbol{V}_s \Gamma) = 0 \tag{8}$$

where we have suppressed the perturbation subscript. Furthermore, the variation in the z direction is far smaller than in the (x, y) plane, so $\nabla_s = \nabla_\perp + O(q)$ and $\boldsymbol{V}_s = \boldsymbol{V}_\perp(z = u) + O(q)$, which implies that this equation can be further simplified to

$$\frac{\partial \Gamma}{\partial t} + \nabla_\perp \cdot (\boldsymbol{V}_\perp(z = u)\Gamma) = 0 \tag{9}$$

where $\nabla_\perp$ and $\boldsymbol{V}_\perp$ are the components parallel to the top and bottom planes for the gradient operator and the fluid velocity, respectively. Note that variables defined on the surface (like u, Γ and S) have no dependency on z, thus $\nabla_\perp$ is equivalent to ∇ for these variables.

Next, let us consider the governing equation for the non-dimensionalized elevation $u \equiv h/d$. In References [4, 11] the leading order equation for elevation $u(x, y, t)$ for the inclined plane problem was obtained from a regular perturbation analysis of the Navier–Stokes equations and the thermal equations. This approach applies similarly to this surfactant problem and we obtain

$$\frac{\partial u}{\partial t} + \nabla \cdot \left(\frac{u^2}{2} \nabla S - \frac{G}{3} u^3 \nabla u + \frac{S}{3} u^3 \nabla \nabla^2 u\right) = 0 \tag{10}$$

where $G \equiv g d^3/\nu\kappa$ is the Galileo number. However, the surface tension is now dependent on not only the temperature T, which is non-dimensionalized by the temperature difference across

the liquid layer ΔT^{p}, but also the surfactant concentration as follows:

$$\begin{aligned}\nabla S &= \nabla\left(\frac{\sigma^{\mathrm{p}}}{\rho\nu\kappa/d}\right)\\ &= \frac{-|\frac{\partial\sigma^{\mathrm{p}}}{\partial T^{\mathrm{p}}}|\Delta T^{\mathrm{p}}}{\rho\nu\kappa/d}\nabla_{\perp}T + \frac{\sigma^{\mathrm{p}}_{\mathrm{eq}}}{\rho\nu\kappa/d}\frac{\partial\sigma}{\partial\Gamma}\nabla\Gamma\end{aligned} \tag{11}$$

For the constitutive model (4), we get

$$\nabla S = -M\nabla_{\perp}T - \alpha E S_{\mathrm{eq}}\frac{\nabla_{\perp}\Gamma}{1-\alpha\Gamma} \tag{12}$$

where $M \equiv \sigma_T \Delta T^{\mathrm{p}}/\rho\gamma\kappa/d$ is the Marangoni number and $\sigma_T = |\partial\sigma^{\mathrm{p}}/\partial T^{\mathrm{p}}|$ is the thermocapillary coefficient. For a vertical thermal conduction temperature profile through the layer as in Reference [11], we have

$$\nabla S = \frac{M(1+F)}{(1+F-Fu)^2}\nabla u - \alpha E S_{\mathrm{eq}}\frac{\nabla\Gamma}{1-\alpha\Gamma} \tag{13}$$

where $F \equiv (1-k_{\mathrm{g}}/k)/(d_{\mathrm{g}}/d + k_{\mathrm{g}}/k)$ with k, k_g the fluid and gas thermal conductivities.

Substituting (13) in (10),

$$\frac{\partial u}{\partial t} + \nabla\cdot\left(\frac{M}{2}\frac{(1+F)u^2}{(1+F-Fu)^2}\nabla u - \frac{G}{3}u^3\nabla u + \frac{S}{3}u^3\nabla\nabla^2 u\right) = \frac{\alpha E S_{\mathrm{eq}}}{2}\nabla\cdot\left(\frac{u^2}{1-\alpha\Gamma}\nabla\Gamma\right) \tag{14}$$

Using the expression for the horizontal velocity (Equation (77) in Reference [11]), the horizontal velocity at the surface $z = u(x, y, t)$ can be written as

$$\boldsymbol{V}_{\perp}(z=u) = (S\nabla\nabla^2 u - G\nabla u)\frac{u^2}{2} + u\nabla S \tag{15}$$

Substituting in (9) and using (13), we get the following pair of coupled equations for (u, Γ):

$$\begin{aligned}&\frac{\partial u}{\partial t} + \nabla\cdot\left(\frac{M}{2}\frac{(1+F)u^2}{(1+F-Fu)^2}\nabla u - \frac{G}{3}u^3\nabla u + \frac{S}{3}u^3\nabla\nabla^2 u\right) = \frac{\alpha E S_{\mathrm{eq}}}{2}\nabla\cdot\left(\frac{u^2}{1-\alpha\Gamma}\nabla\Gamma\right)\\ &\frac{\partial\Gamma}{\partial t} + \nabla\cdot\left[\left(M\frac{(1+F)u}{(1+F-Fu)^2}\nabla u - \frac{G}{2}u^2\nabla u + \frac{S}{2}u^2\nabla\nabla^2 u\right)\Gamma\right] = \alpha E S_{\mathrm{eq}}\nabla\cdot\left(\frac{u\Gamma}{1-\alpha\Gamma}\nabla\Gamma\right)\end{aligned} \tag{16}$$

This pair of equations provides a fairly general model for the thin layer problem with surfactant monolayer under the stated assumptions. However, in the next section we will simplify the model further for the dilute concentration case implemented in the numerical studies in Part II.

2.3. Dilute model

Up to this point in the derivation, the full non-linear constitutive model for surfactant capillarity has been utilized. This covers a wide range of α values. However, we are particularly

interested in the dilute concentration situation, so the constitutive model can be further simplified using $0 \leqslant \alpha \ll 1$ so that we have $S = S_{\mathrm{eq}} + O(\alpha)$ and $1/(1-\alpha\Gamma) = 1 + O(\alpha)$. Equations (16) for (u, Γ) then simplify to

$$\begin{aligned} \frac{\partial u}{\partial t} + \boldsymbol{\nabla} \cdot \left(\frac{M}{2} \frac{(1+F)u^2}{(1+F-Fu)^2} \boldsymbol{\nabla} u - \frac{G}{3} u^3 \boldsymbol{\nabla} u + \frac{S_{\mathrm{eq}}}{3} u^3 \boldsymbol{\nabla} \nabla^2 u \right) &= \frac{\alpha E S_{\mathrm{eq}}}{2} \boldsymbol{\nabla} \cdot \left(u^2 \boldsymbol{\nabla} \Gamma \right) \\ \frac{\partial \Gamma}{\partial t} + \boldsymbol{\nabla} \cdot \left[\left(\frac{M(1+F)u}{(1+F-Fu)^2} \boldsymbol{\nabla} u - \frac{G}{2} u^2 \boldsymbol{\nabla} u + \frac{S_{\mathrm{eq}}}{2} u^2 \boldsymbol{\nabla} \nabla^2 u \right) \Gamma \right] &= \alpha E S_{\mathrm{eq}} \boldsymbol{\nabla} \cdot (u \Gamma \boldsymbol{\nabla} \Gamma) \end{aligned} \tag{17}$$

Rescaling x by L/d so that $x \equiv x^{\mathrm{p}}/L$, and t by $3/G(L/d)^2$ so that $t \equiv t^{\mathrm{p}}/3(L^2/\kappa/G)$, these equations become

$$\begin{aligned} \frac{\partial u}{\partial t} + \boldsymbol{\nabla} \cdot \left(\frac{3}{2} \frac{D(1+F)u^2}{(1+F-Fu)^2} \boldsymbol{\nabla} u - u^3 \boldsymbol{\nabla} u + \frac{u^3}{B} \boldsymbol{\nabla} \nabla^2 u \right) &= \frac{3}{2} D_{\mathrm{s}} \boldsymbol{\nabla} \cdot \left(u^2 \boldsymbol{\nabla} \Gamma \right) \\ \frac{\partial \Gamma}{\partial t} + \boldsymbol{\nabla} \cdot \left[3 \left(\frac{D(1+F)u}{(1+F-Fu)^2} \boldsymbol{\nabla} u - \frac{u^2}{2} \nabla u + \frac{u^2}{2B} \boldsymbol{\nabla} \nabla^2 u \right) \Gamma \right] &= 3 D_{\mathrm{s}} \boldsymbol{\nabla} \cdot (u \Gamma \boldsymbol{\nabla} \Gamma) \end{aligned} \tag{18}$$

where $D = M/G = \sigma_T \Delta T^{\mathrm{p}}/\rho g d^2$ is the inverse dynamic bond number, $B \equiv \rho g L^2/\sigma_{\mathrm{eq}}^{\mathrm{p}}$ is the static bond number, $D_{\mathrm{s}} \equiv \alpha E \sigma_{\mathrm{eq}}^{\mathrm{p}}/\rho g d^2$ is a dimensionless parameter measuring the ratio of the gravity time scale to the surfactant capillarity time scale: $D_{\mathrm{s}} = t_{\mathrm{grav}}^2/t_{\mathrm{surf-cap}}^2 = (d/g)/(\rho d^3/\alpha E \sigma_{\mathrm{eq}}^{\mathrm{p}})$.

To simplify notation for the following stability analysis we set,

$$\begin{aligned} a(u) &\equiv \frac{3}{2} \frac{D(1+F)u^2}{(1+F-Fu)^2} - u^3 \\ b(u) &\equiv \frac{u^3}{B} \\ \boldsymbol{C}(u) &\equiv \left(\frac{3D(1+F)u}{(1+F-Fu)^2} - \frac{3}{2} u^2 \right) \boldsymbol{\nabla} u + \frac{3}{2} \frac{u^2}{B} \boldsymbol{\nabla} \nabla^2 u \\ \kappa_u(u) &\equiv \frac{3}{2} D_{\mathrm{s}} u^2 \\ \kappa_\Gamma(u) &\equiv 3 D_{\mathrm{s}} u \Gamma \end{aligned} \tag{19}$$

Then (18) can be rewritten more compactly as

$$\begin{aligned} \frac{\partial u}{\partial t} + \boldsymbol{\nabla} \cdot (a(u) \boldsymbol{\nabla} u + b(u) \boldsymbol{\nabla} \nabla^2 u) &= \boldsymbol{\nabla} \cdot (\kappa_u(u) \boldsymbol{\nabla} \Gamma) \\ \frac{\partial \Gamma}{\partial t} + \boldsymbol{\nabla} \cdot [\boldsymbol{C}(u) \Gamma] &= \boldsymbol{\nabla} \cdot (\kappa_\Gamma(u, \Gamma) \boldsymbol{\nabla} \Gamma) \end{aligned} \tag{20}$$

We develop a linear stability analysis for this system in the next section, and give numerical results for some relevant test problems in Part II.

3. STABILITY ANALYSIS

Assume a perturbation around the stationary state $u=1,\ \Gamma=1$ of the form

$$\begin{aligned} u(x,y,t) &= 1+\delta u = 1+\Sigma_p \eta_p e^{\gamma_p t} e^{i2\pi \boldsymbol{p}\cdot\boldsymbol{x}} \\ \Gamma(x,y,t) &= 1+\delta\Gamma = 1+\Sigma_q \xi_q e^{\lambda_q t} e^{i2\pi \boldsymbol{q}\cdot\boldsymbol{x}} \end{aligned} \tag{21}$$

where the wavevectors are $\boldsymbol{p}=p_x\boldsymbol{e}_x+p_y\boldsymbol{e}_y$, $\boldsymbol{q}=q_x\boldsymbol{e}_x+q_y\boldsymbol{e}_y$, the wavenumbers are $p=\sqrt{p_x^2+p_y^2}$, $q=\sqrt{q_x^2+q_y^2}$, and the position vector is $\boldsymbol{x}=x\boldsymbol{e}_x+y\boldsymbol{e}_y$.

Linearizing Equations (20) around $u=1,\ \Gamma=1$, we obtain

$$\begin{aligned} \frac{\partial \delta u}{\partial t} + \boldsymbol{\nabla}\cdot(a(1)\boldsymbol{\nabla}\delta u + b(1)\boldsymbol{\nabla}\nabla^2\delta u) &= \boldsymbol{\nabla}\cdot(\kappa_u(1)\boldsymbol{\nabla}\delta\Gamma) \\ \frac{\partial \delta\Gamma}{\partial t} + \boldsymbol{\nabla}\cdot(\delta\boldsymbol{C}_\Gamma) &= \boldsymbol{\nabla}\cdot(\kappa_\Gamma(1,1)\boldsymbol{\nabla}\delta\Gamma) \end{aligned} \tag{22}$$

for the perturbation pair in (21),where $\delta\boldsymbol{C}_\Gamma=(3D(1+F)-\frac{3}{2})\boldsymbol{\nabla}\delta u+(3/2B)\boldsymbol{\nabla}\nabla^2\delta u$, $\kappa_u(1)=\frac{3}{2}D_s$ and $\kappa_\Gamma(1,1)=3D_s$.

Introducing the Fourier expansions for δu, $\delta\Gamma$, in (22)

$$\begin{aligned} &\Sigma_p\eta_p\left[\gamma_p+4\pi^2p^2\left(-\frac{3}{2}D(1+F)+1+\frac{4\pi^2p^2}{B}\right)\right]e^{\gamma_p t}e^{i2\pi\boldsymbol{p}\cdot\boldsymbol{x}} \\ &\quad=\Sigma_q-6\pi^2q^2D_s\xi_q e^{\lambda_q t}e^{i2\pi\boldsymbol{q}\cdot\boldsymbol{x}} \\ &\Sigma_q\xi_q\lambda_q e^{\lambda_q t}e^{i2\pi\boldsymbol{q}\cdot\boldsymbol{x}}+\Sigma_p 6\pi^2p^2\left(-2D(1+F)+1+\frac{4\pi^2p^2}{B}\right)\eta_p e^{\gamma_p t}e^{i2\pi\boldsymbol{p}\cdot\boldsymbol{x}} \\ &\quad=\Sigma_q-12\pi^2q^2D_s\xi_q e^{\lambda_q t}e^{i2\pi\boldsymbol{q}\cdot\boldsymbol{x}} \end{aligned} \tag{23}$$

Collecting terms,

$$\begin{aligned} \gamma_q &= \lambda_q \\ \gamma_q+6\pi^2q^2D_s\left(\frac{\xi_q}{\eta_q}\right)+4\pi^2q^2\left(-\frac{3}{2}D(1+F)+1+\frac{4\pi^2q^2}{B}\right)&=0 \\ \lambda_q+6\pi^2q^2\left(-2D(1+F)+1+\frac{4\pi^2q^2}{B}\right)\left(\frac{\xi_q}{\eta_q}\right)^{-1}+12\pi^2q^2D_s&=0 \end{aligned} \tag{24}$$

for all $\boldsymbol{q} = (1,0),(0,1),(1,1),\ldots$. Setting

$$\begin{aligned}
\hat{a} &\equiv 6\pi^2 q^2 D_s \\
\hat{b} &\equiv 4\pi^2 q^2 \left(1 + \frac{4\pi^2 q^2}{B}\right) \\
\hat{c} &\equiv 6\pi^2 q^2 D(1+F) \\
\hat{x} &\equiv \lambda_q \\
\hat{y} &\equiv \frac{\xi_q}{\eta_q}
\end{aligned} \tag{25}$$

for algebraic convenience, then (24) reduces to a pair of non-linear algebraic equations

$$\begin{aligned}
\hat{x} + \hat{a}\hat{y} + \hat{b} - \hat{c} &= 0 \\
\hat{x} + \left(\frac{3}{2}\hat{b} - 2\hat{c}\right)\hat{y}^{-1} + 2\hat{a} &= 0
\end{aligned} \tag{26}$$

which admits two pairs of solutions

$$\begin{aligned}
\hat{x}_{1,2} &= \frac{-2\hat{a} + (\hat{c} - \hat{b}) \pm \sqrt{(2\hat{a} + \hat{b} - \hat{c})^2 - 2\hat{a}\hat{b}}}{2} \\
\hat{y}_{1,2} &= \frac{2\hat{a} + (\hat{c} - \hat{b}) \mp \sqrt{(2\hat{a} + \hat{b} - \hat{c})^2 - 2\hat{a}\hat{b}}}{2\hat{a}}
\end{aligned} \tag{27}$$

or equivalently in terms of γ_q and ξ_q/η_q using the notations in (25):

$$\begin{aligned}
(\gamma_q)_{1,2} = (\lambda_q)_{1,2} &= 2\pi^2 q^2 \left(\varepsilon_q - 3D_s \pm \sqrt{\Delta_q}\right) \\
\left(\frac{\xi_q}{\eta_q}\right)_{1,2} &= 1 + \frac{\varepsilon_q}{3D_s} \mp \frac{1}{3D_s}\sqrt{\Delta_q}
\end{aligned} \tag{28}$$

where

$$\Delta_q \equiv (\varepsilon_q - 3D_s)^2 - 3D_s\left(1 + \frac{4\pi^2 q^2}{B}\right) \tag{29}$$

and

$$\varepsilon_q = \frac{3D(1+F)}{2} - 1 - \frac{4\pi^2 q^2}{B} \tag{30}$$

The existence of two solution pairs suggests that the Fourier series expansion of u and Γ should be rewritten as

$$\begin{aligned}
u(x,y,t) &= 1 + \delta u = 1 + \Sigma_q(\eta_{q1} e^{\gamma_{q1} t} + \eta_{q2} e^{\gamma_{q2} t}) e^{i2\pi \boldsymbol{q}\cdot\boldsymbol{x}} \\
\Gamma(x,y,t) &= 1 + \delta\Gamma = 1 + \Sigma_q \left(\left(\frac{\xi_q}{\eta_q}\right)_1 \eta_{q1} e^{\gamma_{q1} t} + \left(\frac{\xi_q}{\eta_q}\right)_2 \eta_{q2} e^{\gamma_{q2} t}\right) \eta_q e^{i2\pi \boldsymbol{q}\cdot\boldsymbol{x}}
\end{aligned} \tag{31}$$

That is, the amplitude of each mode involves two different time-dependent components where the coefficients η_{q1} and η_{q2} can be determined from the initial state of u and Γ collectively. We consider these respective cases in Sections 3.1 and 3.2 and then also examine the limiting case when the diffusion approaches 0. This then leads to a convenient categorization of the solution regimes in terms of parameter ε_q in (30).

To study the linear stability of the qth mode in Equation (31), it is convenient to distinguish the cases where $\Delta_q < 0$ from $\Delta_q \geqslant 0$, because this distinction determines whether $(\gamma_q)_{1,2}$ are real or complex. In turn, this determines whether the qth mode is convective or diffusive.

3.1. $\Delta_q < 0$

By (29), $\Delta_q < 0$ is equivalent to

$$3D_s - \sqrt{3D_s\left(1 + \frac{4\pi^2 q^2}{B}\right)} < \varepsilon_q < 3D_s + \sqrt{3D_s\left(1 + \frac{4\pi^2 q^2}{B}\right)} \tag{32}$$

and implies both $(\gamma_q)_{1,2}$ and $(\xi_q/\eta_q)_{1,2}$ are complex. As a result, the qth mode of $u(x,t)$ in (31) is composed of two waves travelling in opposite directions:

$$\eta_{q1} e^{2\pi^2 q^2(\varepsilon_q - 3D_s)t} e^{i2\pi\left(\boldsymbol{q}\cdot\boldsymbol{x} + \pi q^2\sqrt{|\Delta_q|}t\right)} \tag{33}$$

and

$$\eta_{q2} e^{2\pi^2 q^2(\varepsilon_q - 3D_s)t} e^{i2\pi\left(\boldsymbol{q}\cdot\boldsymbol{x} - \pi q^2\sqrt{|\Delta_q|}t\right)} \tag{34}$$

with period

$$\tau_q = \frac{1}{\pi q^2\sqrt{|\Delta_q|}} \tag{35}$$

The amplitude of these travelling waves for u grows/decays exponentially with rate given by

$$\lambda_q = 2\pi^2 q^2(\varepsilon_q - 3D_s) \tag{36}$$

Similarly the two travelling waves for the qth mode of $\Gamma(x,t)$ are

$$\left(1 + \frac{\varepsilon_q}{3D_s} - i\frac{\sqrt{|\Delta_q|}}{3D_s}\right)\eta_{q1} e^{2\pi^2 q^2(\varepsilon_q - 3D_s)t} e^{i2\pi\left(\boldsymbol{q}\cdot\boldsymbol{x} + \pi q^2\sqrt{|\Delta_q|}t\right)} \tag{37}$$

and

$$\left(1 + \frac{\varepsilon_q}{3D_s} + i\frac{\sqrt{|\Delta_q|}}{3D_s}\right)\eta_{q2} e^{2\pi^2 q^2(\varepsilon_q - 3D_s)t} e^{i2\pi\left(\boldsymbol{q}\cdot\boldsymbol{x} - \pi q^2\sqrt{|\Delta_q|}t\right)} \tag{38}$$

Note that the phase angle for the qth mode of $\Gamma(x,t)$ lags behind that of $u(x,t)$ by

$$\phi_q = \tan^{-1}\left(\frac{\sqrt{|\Delta_q|}}{3D_s + \varepsilon_q}\right) \tag{39}$$

and the ratio of its amplitude to that of $u(x,t)$ is

$$r_q = \sqrt{\left(1 + \frac{\varepsilon_q}{3D_s}\right)^2 + \frac{|\Delta_q|}{9D_s^2}} \tag{40}$$

It follows that the amplitude of the qth mode of both $u(x,t)$ and $\Gamma(x,t)$ should be attenuated when $\varepsilon_q - 3D_s < 0$, and amplified when $\varepsilon_q - 3D_s > 0$.

3.2. $\Delta_q \geqslant 0$

By (29), $\Delta_q \geqslant 0$ is equivalent to

$$\varepsilon_q \leqslant 3D_s - \sqrt{3D_s\left(1 + \frac{4\pi^2 q^2}{B}\right)} \tag{41}$$

or

$$\varepsilon_q \geqslant 3D_s + \sqrt{3D_s\left(1 + \frac{4\pi^2 q^2}{B}\right)} \tag{42}$$

and both $(\gamma_q)_{1,2}$ and $(\xi_q/\eta_q)_{1,2}$ are real, which implies that the qth modes of $u(x,y,t)$ and $\Gamma(x,y,t)$ are diffusive. In addition, it can be easily verified from (28) that

$$\varepsilon_q \leqslant 3D_s - \sqrt{3D_s\left(1 + \frac{4\pi^2 q^2}{B}\right)} \Rightarrow (\gamma_q)_{1,2} \leqslant 0 \tag{43}$$

and

$$\varepsilon_q \geqslant 3D_s + \sqrt{3D_s\left(1 + \frac{4\pi^2 q^2}{B}\right)} \Rightarrow (\gamma_q)_{1,2} \geqslant 0 \tag{44}$$

Hence, unlike in the oscillatory parametric region, the signs of $Re((\gamma_q)_{1,2})$ do not change in each of the two non-oscillatory parametric regions. Furthermore, reasoning as in the discussion of the case $\Delta_q < 0$, we can conclude that $\varepsilon_q - 3D_s$ has the same sign as $Re((\gamma_q)_{1,2})$, irrespective of the sign of Δ_q. Thus $\varepsilon_q = 3D_s$ defines the division between the stable and unstable parameter regions.

However, unlike the situation for the previous oscillatory parameter region discussed in Section 3.1, the exponential growth rate for the qth modes of u and Γ now can take two values. According to (28), they are

$$\lambda_{q1} = 2\pi^2 q^2 \left(\varepsilon_q - 3D_s + \sqrt{\Delta_q}\right) \tag{45}$$

and

$$\lambda_{q2} = 2\pi^2 q^2 \left(\varepsilon_q - 3D_s - \sqrt{\Delta_q}\right) \tag{46}$$

The amplitude ratio of the qth mode of Γ versus that of u (compare (40)) correspondingly takes the two values

$$r_{q1} = 1 + \frac{\varepsilon_q}{3D_s} - \frac{\sqrt{\Delta_q}}{3D_s} \tag{47}$$

and

$$r_{q2} = 1 + \frac{\varepsilon_q}{3D_s} + \frac{\sqrt{\Delta_q}}{3D_s} \tag{48}$$

It can be shown that

$$\lambda_{q1} \geqslant \lambda_{q2} \geqslant 0 \quad \text{or} \quad 0 \geqslant \lambda_{q1} \geqslant \lambda_{q2} \tag{49}$$

with the equalities holding if and only if $\Delta_q = (\varepsilon_q - 3D_s)^2 - 3D_s(1 + (4\pi^2 q^2/B)) = 0$. This implies λ_{q1} corresponds to the faster time scale when the system is unstable, and to the slower time scale when the system is stable. In either case, the (λ_{q1}, r_{q1}) component of the qth mode will dominate the (λ_{q2}, r_{q2}) component as $t \to \infty$, particularly when $\Delta_q \gg 1$ or $q \gg 1$.

3.3. *The limit* $D_s \to 0$

When $D_s \to 0$, the coupling between the surface elevation and the surfactant concentration degenerates from two-way to one-way: the surface elevation is not affected by the surfactant concentration whereas the surfactant is still advected by the surface velocity due to the thermocapillary stress and the surface tension. Moreover, it can be verified from (28) that when $D_s \to 0$, $\Delta_q = \varepsilon_q^2 \geqslant 0$. Therefore this class falls in the non-oscillatory parameter region. From the discussion in the previous subsection, we know that for the qth mode, there are two components growing at different exponential rates. Of the two $(\lambda_q, \xi_q/\eta_q)$ solution pairs in (28), one is singular in the limit for $D_s \to 0$ whereas the other is not. Considering the limit, the solution to the degenerate form of the equations is

$$\begin{aligned} \lambda_q &= 4\pi^2 q^2 \varepsilon_q \\ \frac{\xi_q}{\eta_q} &= \frac{3}{2} + \frac{3D(1+F)}{4\varepsilon_q} \end{aligned} \tag{50}$$

This solution can be physically interpreted as follows: $\nabla \delta u$ and $\nabla \nabla^2 \delta u$ contribute to the convection velocity for Γ, and thus $\delta\Gamma$ grows at the same exponential rate as δu. If δu decays, so does $\delta\Gamma$; thus u and Γ will eventually reach stationary profiles. If δu continues to grow larger, then $\delta\Gamma$ will also grow larger, but remain proportional to δu. If δu is not attenuated nor amplified, then Γ will be continuously convected by a constant velocity. Eventually the ratio of $\delta\Gamma$ versus δu will approach infinity, which explains the singularity in ξ_q/η_q at $\varepsilon_q = 0$ in (50).

The limit form of (24) has one pair of solutions, whereas there are two pairs of solutions in (28), which implies one pair will be singular and thus invalid when $D_s \to 0$. The limits of the two pairs of solutions (27) are

$$\begin{aligned} \lim_{\varepsilon_q \to 0} (\lambda_q)_{1,2} &= 2\pi^2 q^2 \left(\varepsilon_q \pm |\varepsilon_q|\right) \\ \lim_{\varepsilon_q \to 0} \left(\frac{\xi_q}{\eta_q}\right)_{1,2} &= \frac{3(\frac{D(1+F)}{2} + \varepsilon_q)}{\varepsilon_q \pm |\varepsilon_q|} \end{aligned} \tag{51}$$

When $\varepsilon_q > 0$, $((\lambda_q)_1, (\xi_q/\eta_q)_1)$ is non-singular and approaches (50) as $D_s \to 0$, whereas when $\varepsilon_q < 0$, $((\lambda_q)_2, (\xi_q/\eta_q)_2)$ is non-singular and approaches (50) as $D_s \to 0$. In either case, for the singular solution pair, $\lambda_q \to 0$ and $\xi_q/\eta_q \to \infty$ as $D_s \to 0$. This implies for the two components of each mode, that the time scale of one of them will approach infinity when $D_s \to 0$, and thus becomes non-physical.

3.4. Categorization of the parameter regions

Based on the discussions in Sections 3.1–3.3, the evolution of the qth mode of (u, Γ) around the stationary state $u = 1, \Gamma = 1$ can be predicted to behave as follows:

- If $\varepsilon_q > 3D_s$, the amplitude of the qth modes of both u and Γ will grow in time; otherwise they will decay in time, either monotonically or periodically. Compared with the $\varepsilon_q > 0$ criteria for the surfactant-free problem [11], it is evident that adding surfactant raises the threshold value of ε_q and thus helps stabilize the surface profile.
- If $\Delta_q \geqslant 0$, the qth mode of both u and Γ evolve monotonically in time at the same exponential rate; otherwise, they evolve periodically with the same frequency, and there is a fixed phase shift between them.

We can physically interpret the monotonic versus periodic (or convective versus diffusive) evolution patterns as follows:

The thermocapillary effect introduces non-uniformity to the surface tension on the interface. The resultant surface velocity then convects the surfactant on the surface. However, because the surfactant-capillary effect lowers the surface tension in the high concentration areas and raises the surface tension in the low concentration areas, the surfactant counters the convective thermocapillary effect. Thus there are two conflicting contributions to the surface velocity. One is present in the original surfactant-free problem. It arises from thermocapillarity, gravity and surface tension and is represented by the convection velocity in the Γ equation in (18). The other is new in this coupled surfactant model. It comes from the surfactant-capillarity and is represented by the diffusion terms on the right-hand side of the u and Γ equations in (18). Note that there is also a latency in the action of the surfactant-capillarity effect to counter the thermocapillary effect. When these two conflicting contributions balance (which corresponds to $\Delta_q < 0$), the surface velocity field undulates between two different distributions and thus the u and Γ profiles evolve periodically. When one of the two contributions dominates the other (which corresponds to $\Delta_q > 0$), the development of the surface velocity field follows the dominant contribution and thus u and Γ evolve monotonically. In either case, as long as thermocapillarity is sufficiently stronger than surfactant-capillarity, that is $\varepsilon_q > 3D_s$, or in other words, as long as a strong enough thermal flux is specified for the system,

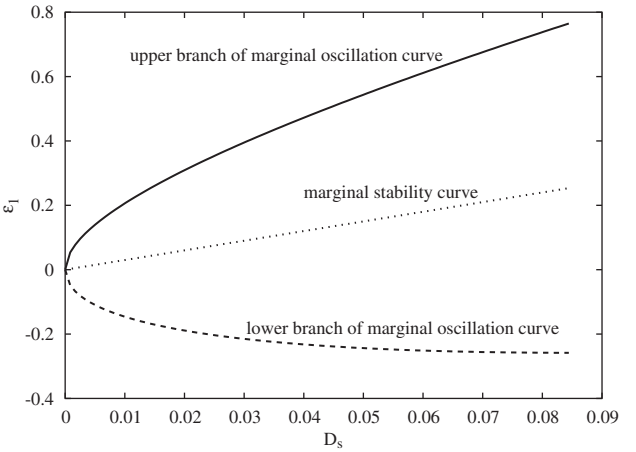

Figure 4. Marginal curves of ε_1 versus D_s.

the amplitude of the surface elevation will be pulled increasingly larger and thus the system becomes unstable.

Applying the results in the previous sections to the leading mode ($q=1$), we can categorize the linear stability of (u,Γ) around the stationary state $u=1,\Gamma=1$ into the following four parameter regions:

Region 1: $\varepsilon_1 > 3D_s$ and $\Delta_1 < 0$. Oscillatory and unstable region. The oscillation period is $1/\pi\sqrt{|\Delta_1|}$, the exponential growth rate of the amplitude of the leading mode is $\lambda_1 = 2\pi^2(\varepsilon_1 - 3D_s)$, the amplitude ratio of the leading mode of Γ versus u is

$$r_1 = \sqrt{\left(1 + \frac{\varepsilon_1}{3D_s}\right)^2 + \frac{|\Delta_1|}{9D_s^2}}$$

and the phase angle of the leading Γ mode lags behind that of u by $\tan^{-1}(\sqrt{|\Delta_1|}/3D_s + \varepsilon_1)$. $\Delta_1 \equiv (\varepsilon_1 - 3D_s)^2 - 3D_s(1 + 4\pi^2/B)$.

Region 2: $\varepsilon_1 > 3D_s$ and $\Delta_1 \geqslant 0$. Non-oscillatory and unstable region. The exponential growth rates of the leading mode of u and Γ are $(\lambda_1)_1 = 2\pi^2(\varepsilon_1 - 3D_s + \sqrt{\Delta_1})$ and $(\lambda_1)_2 = 2\pi^2(\varepsilon_1 - 3D_s - \sqrt{\Delta_1})$, and the corresponding ratios of the leading mode of Γ versus u are $(r_1)_1 = 1 + (\varepsilon_1/3D_s) - (\sqrt{\Delta_1}/3D_s)$ and $(r_1)_2 = 1 + (\varepsilon_1/3D_s) + (\sqrt{\Delta_1}/3D_s)$.

Region 3: $\varepsilon_1 < 3D_s$ and $\Delta_1 < 0$. Oscillatory and stable region. The expressions for the oscillation period, amplitude growth rate, amplitude ratio and phase shift are the same as in region 1.

Region 4: $\varepsilon_1 < 3D_s$ and $\Delta_1 \geqslant 0$. Non-oscillatory and stable region. The expressions for the amplitude growth rate and ratio are the same as in region 2.

Figure 4 shows two curves that partition the parameter plane (ε_1, D_s) into the four parameter regions above. The marginal oscillation curve is defined as $\Delta_1(\varepsilon_1, D_s) = 0$. It consists of two

branches

$$(\varepsilon_1)_1 = 3D_s + \sqrt{3D_s\left(1+\frac{4\pi^2}{B}\right)}$$
$$(\varepsilon_1)_2 = 3D_s - \sqrt{3D_s\left(1+\frac{4\pi^2}{B}\right)} \tag{52}$$

which are depicted as the upper(solid line) and lower(dotted line) branches respectively in the figure. The marginal stability curve is defined as $Re(\lambda_1(\varepsilon_1, D_s)) = 0$, which is simply the straight line $\varepsilon_1 = 3D_s$ in the figure.

In Part II we develop a finite element formulation and investigate the non-linear stability behaviour numerically.

4. CONCLUSIONS

In this study we have investigated model development, scaling and perturbation analysis for problems concerning long wavelength evolution of heated thin liquid films including the effect of a surfactant monolayer. The key physical feature studied here is the role of surface tension in these thin layer problems and the competitive nature of the respective thermal and chemical effects. Elsewhere we have also extended the treatment of the heated layer problem to include plane inclination at a small angle and found from the time dependent numerical solutions that a slight inclination of the system may give rise to premature onset of instability [11]. Of particular interest in the present work is the combined effect of thermocapillarity and the surfactant on the stability of the layer. The monolayer surfactant model involves an additional transport equation for surfactant concentration on the surface. A stability analysis is carried out for the first time to identify the oscillatory/non-oscillatory,and stable/unstable parametric regions. Later, in Part II we construct a finite element formulation and algorithm that are implemented to explore the stability regimes.

ACKNOWLEDGEMENTS

We would like to extend our appreciation to Dr Van Nguyen for several very stimulating discussions on the behaviour and properties of monolayer surfactants and for providing several key references that were helpful in the present modelling investigation.

REFERENCES

1. Gaines Jr GL. *Insoluble Monolayers at Liquid–Gas Interfaces*. Wiley: New York, 1966.
2. Shivamoggi BK. *Theoretical Fluid Dynamics*. Wiley: New York, 1998.
3. Davis SH. Thermocapillary instabilities. *Annual Review of Fluid Mechanics* 1987; **19**:403–435.
4. VanHook SJ, Schatz MF, Swift JB, McCormick WD, Swinney HL. Long-wavelength surface-tension-driven Bénard convection: experiment and theory. *Journal of Fluid Mechanics* 1997; **345**:45–78.
5. VanHook SJ. Long-wavelength instability in surface-tension-driven Bénard convection. *Ph.D. Dissertation*, University of Texas, Austin, 1996.
6. Schatz MF, VanHook SJ, McCormick WD, Swift JB, Swinney HL. Onset of surface-tension driven Bénard convection. *Physics Review Letters* 1995; **75**(10):1938–1941.
7. Schatz MF, VanHook SJ, McCormick WD, Swift JB, Swinney HL. Time-independent square patterns in surface-tension-driven Bénard convection. *Physics of Fluids* 1999; **11**(9):2577–2582.

8. Smith KA. On convective instability induced by surface-tension gradients. *Journal of Fluid Mechanics* 1966; **24**(2):401–414.
9. Levich V. *Physicochemical Hydrodynamics*. Prentice-Hall: Englewood Cliffs, NJ, 1962.
10. VanHook SJ, Schatz MF, McCormick WD, Swift JB, Swinney HL. Long-wavelength instability in surface-tension-driven Bénard convection. *Physics Review Letters* 1995; **75**(24):4397–4400.
11. Wang X, Carey GF. Finite element study of a heated thin fluid layer. *Numerical Heat Transfer* 2004; **45**(9):841–867.
12. Grotberg JB, Gaver III DP. A synopsis of surfactant spreading research. *Journal of Colloid and Interface Science* 1996; **178**:377–378.
13. Eggleton CD, Tsai T, Stebe KJ. Tip streaming from a drop in the presence of surfactants. *Physics Review Letters* 2001; **87**(4):048302.
14. Eggleton CD, Stebe KJ. An adsorption–desorption-controlled surfactant on a deforming droplet. *Journal of Colloid and Interface Science* 1998; **208**:68–80.
15. Eggleton CD, Pawar YP, Stebe KJ. Insoluble surfactants on a drop in an extensional flow: a generalization of the stagnated surface limit to deforming interfaces. *Journal of Fluid Mechanics* 1999; **385**:79–99.
16. Williams HAR. Two-dimensional surfactant-driven flows of thin liquid films. *Ph.D. Dissertation*, Cambridge University, 1998.
17. Matar OK, Troian SM. Spreading of a surfactant monolayer on a thin liquid film: onset and evolution of digitated structures. *Chaos* 1999; **9**(1):141–153.
18. Oron A, Davis SH, Bankoff SG. Long-scale evolution of thin liquid films. *Reviews of Modern Physics* 1997; **69**(3):931–980.

